Intermetallic Formation on the Fracture of Sn/Pb Solder and Pd/Ag Conductor Interfaces

BI-SHIO CHIOU, K. C. LIU, JENQ-GONG DUH, AND P. SAMY PALANISAMY

Abstract—**Intermetallic formation between thick film mixed bonded conductor and Sn/Pb solder is investigated. Microstructural evolution of the interfacial morphology, elemental and phase distribution is probed with the aid of electron microscopy and X-ray diffraction. There exists mechanical interlocking between conductor and substrate. Penetration of a Bi element into the substrate is observed. A decrease in adhesion strength occurs when the sample is aged at 130°C for a long period of time. Microstructural analysis reveals the segregation of Pb-rich and Sn-rich phases in aged samples and formation of intermetallic compounds Pd_3Sn_2, Pd_2Sn, Pd_3Sn_2, PdSn, Ag_5Sn, and Ag_3Sn. It is argued that conductor swelling caused by tin diffusion into the conductor film and volume change resulting from the intermetallic formation are major factors in the degradation of the peel strength.**

I. Introduction

TIN/LEAD solders are commonly used in the electronic industry as interconnects and bonding pads for microcircuits. During the soldering operation and subsequent joint life, intermetallic compounds form and grow. The formation of the intermetallic compound may cause mechanical failure during thermal or power cycle [1]–[4]. Microcircuit performance and lifetime are then degraded as these intermetallics grow. However, kinetics of the intermetallic growth and the effect of the intermetallic compounds on the physical and mechanical properties of solder joints are not yet well understood.

The purpose of this research is to study the effect of intermetallic formation on the fracture of a 63/37 Sn/Pb solder and Pd/Ag thick film conductor. Palladium/silver-based conductors are probably the most commonly used inks in the technology thick film hybrid circuits. The commercial significance of Sn/Pb solder and Pd/Ag conductor in the electronic industry requires a better understanding of this material system. The microstructural evolution of the interfacial morphology is probed with the aid of electron microscopy and X-ray diffraction.

II. Experimental Procedure

A. Sample Preparation

Two commercial Dupont Pd/Ag conductor pastes, and a 63/37 Sn/Pb[1] solder are employed in this paper. The test pattern, shown in Fig. 1, was printed on 96% Al_2O_3 substrate[2] and dried at 150°C for 15 min. Samples were then air fired in a belt furnace. The total firing cycle time at 32 min with 7 min of peak firing at 850°C. Adhesion was evaluated by use of a wire/peel test. Four wires of 0.8-mm diameter were placed on every substrate crossing each pad. The wires were lined up with the three pattern features and the loop on the bottom edge. The loop was clipped after the soldering process. Test samples were then stored at 135°C for 0, 40, 100, 210, 400, and 600 h. Wires were bent 90° before the adhesion test. The adhesion strength was determined by pulling the wire using an Instron machine with a strain rate of 26.2 mm/min or 2.28 mm/min. The fracture mode of the test specimens was examined.

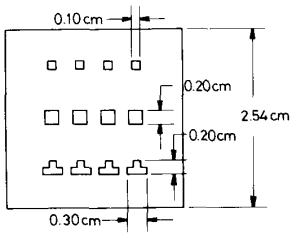

Fig. 1. Conductor test pattern employed in this study.

B. Analysis and Characterization

Compositions of the conductors employed in this study were analyzed with an Atomic Emission Spectrometer (AES, GVM-1000P, Schimadzu, Japan) and an X-ray diffractometer (XRD, D/MAX-B, Rigaku, Japan). Microstructure and elemental distribution of the specimens were investigated with a scanning electron microscope (SEM, S250MK3, Cambridge, England) and an electron probe microanalyzer (EPMA, JCXA-733, JEOL, Japan). Oxidation state of some conductor constituents was identified with ESCA (Electron Spectroscopy for Chemical Analysis, Perkin-Elmer PHI 1905, Minnesota).

III. Results and Discussion

A. Characteristics of the Conductor

Two Dupont mixed bonded Pd/Ag conductors, designated as DC1 and DC2, are employed in this paper. The Pd/Ag ratios and the major constituents of these two conductors are identified by X-ray diffraction and AES, respectively. The cell constant, a, obtained from XRD experiments versus the Nelson–Riley function, $(\cos^2\theta/\sin\theta+\cos^2\theta/\theta)$ [5], for two conductors are plotted in Figs. 2 and 3. The least square fitting

Manuscript received May 12, 1989; revised September 12, 1989.

B.-S. Chiou is with the Institute of Electronics, National Chiao Tung University, Hsinchu, Taiwan.

K. C. Liu and J.-G. Duh are with the Department of Materials Science and Engineering, National Tsing Hua University, Hsinchu, Taiwan.

P. S. Palanisamy is with Delco Electronics, General Motor Corporation, Kokomo, IN 46902.

IEEE Log Number 8932944.

[1] Multicore Soldering Technology Ltd.

[2] AlSiMag 614, 3M Co.

0148-6411/90/0600-0267$01.00

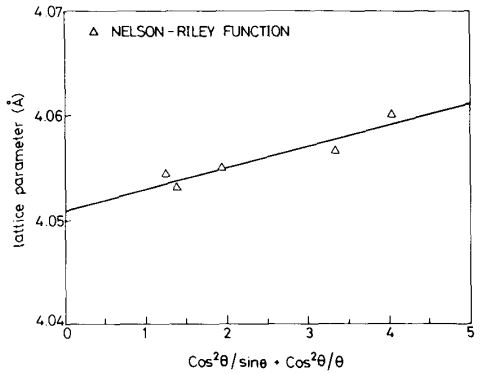

Fig. 2. Lattice parameter versus Nelson-Riley function for conductor DC1.

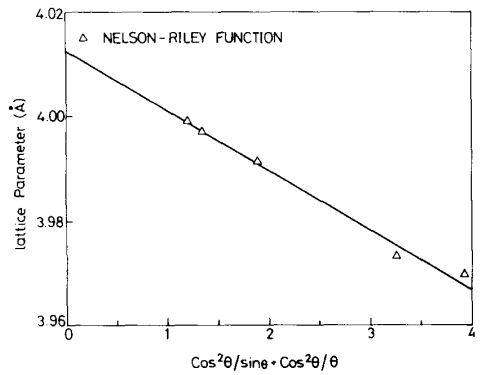

Fig. 3. Lattice parameter versus Nelson-Riley function for conductor DC2.

of the two linear plots are

$$\text{conductor DC1: } a = 4.05 + 2.036 \times 10^{-3} \cdot \left(\frac{\cos^2\theta}{\sin\theta} + \frac{\cos^2\theta}{\theta}\right) \quad (1)$$

$$\text{conductor DC2: } a = 4.01 - 0.00113\left(\frac{\cos^2\theta}{\sin\theta} + \frac{\cos^2\theta}{\theta}\right) \quad (2)$$

where θ is the diffraction angle corresponding to a Cu target.

The lattice parameters, which are the intercepts in Figs. 2 and 3, are 4.05 Å and 4.01 Å for conductors DC1 and DC2, respectively. Values of Pd:Ag ratios were determined as 1:8.09 and 1:2.33, respectively, for DC1 and DC2, on the basis of the associated correlation of the lattice parameter in Pd-Ag solid solution [6].

Pd:Ag ratios can also be determined from the ratio of the area under (111) peak in Figs. 4 and 5 of the X-ray profile. Pd:Ag ratios thus obtained are 1:7.5 for DC1 and 1:2.99 for DC2. AES results on the major constituents of DC1 and DC2 are summarized in Table I, which indicates that conductor DC2 has higher Pd content than DC1 does. The average Pd:Ag ratio is 1:8 for DC1 and 1:3 for DC2. It appears that Pd:Ag ratios evaluated by three different methods are fairly comparable.

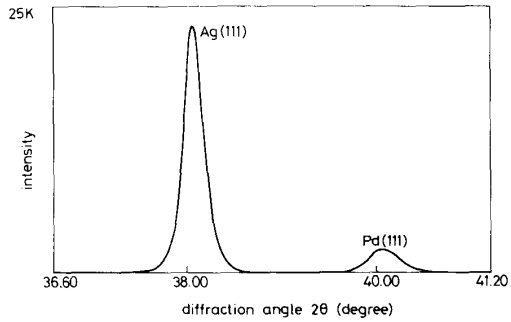

Fig. 4. X-ray diffraction pattern of conductor DC1.

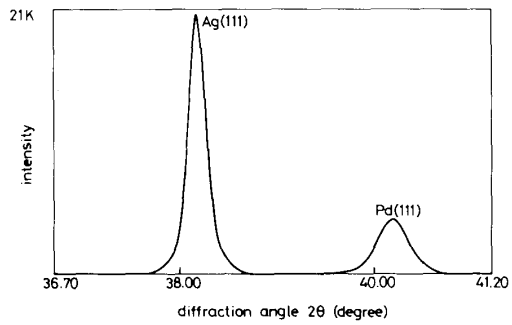

Fig. 5. X-ray diffraction pattern of conductor DC2.

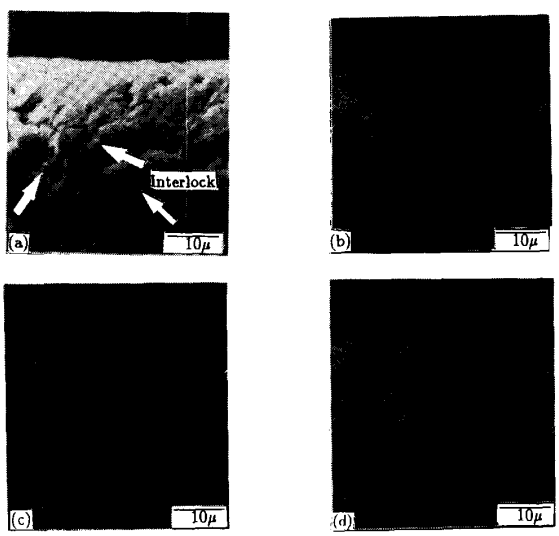

Fig. 6. Cross-sectional SEM micrograph and X-ray mapping of as fired conductor DC2. (a) SEI. (b) Ag X-ray mapping. (c) Pd X-ray mapping. (d) Bi X-ray mapping.

TABLE I
AES RESULTS ON MAJOR CONSTITUENTS OF CONDUCTORS DC1 AND DC2

	Pd	Ag	Pb	Bi	Cu	Pd:Ag
	(Relative Concentration)*					
DC1	1036.4	8963.6	177.2	1242.4	6.67	1:8.65
DC2	2242.2	7757.8	152.1	1008.9	4.78	1:3.46

* Normalized to Pd + Ag = 10000

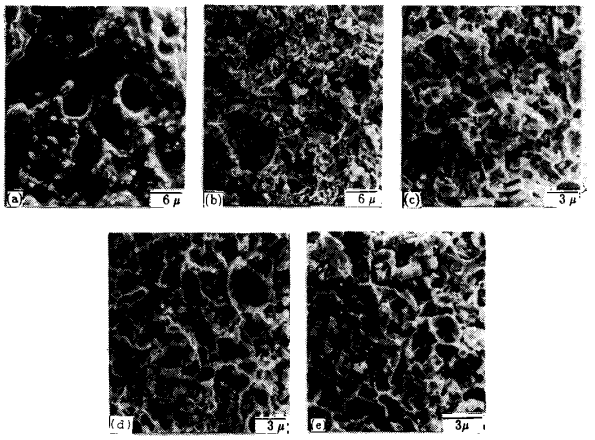

Fig. 7. Fracture surface of conductor DC1 after various time of aging at 130°C. (a) 0 h. (b) 40 h. (c) 100 h. (d) 210 h. (e) 400 h. Fracture occurs at the conductor/solder interface.

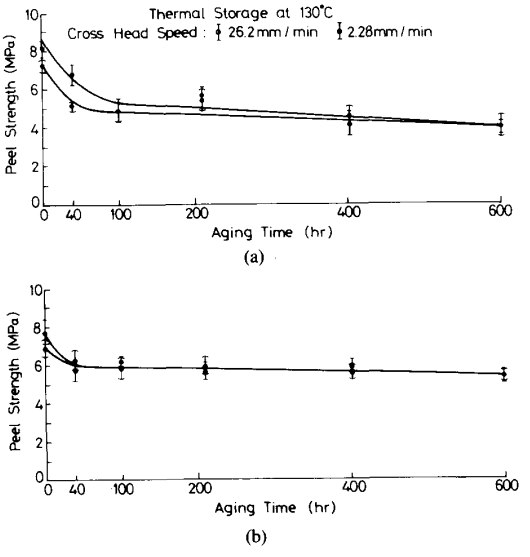

Fig. 8. Peel strength as a function of aging time for conductor (a) DC1 and (b) DC2.

TABLE II
FAILURE MODE OF CONDUCTORS AFTER PEEL TEST

Conductor DC1		Fracture Mode		
Aging Time at 130°C (hr)	Strain rate mm/min	A	B	C
0	26.2		12/12*	
	2.28		9/12	3/12
40	26.2		8/8	
	2.28		8/8	
100	26.2	5/8	3/8	
	2.28	4/8	4/8	
210	26.2	6/12	6/12	
	2.28		8/8	
402	26.2	7/8	1/8	
	2.28	4/8	4/8	
600	26.2		8/8	
	2.28		8/8	

Conductor DC2		Fracture Mode		
Aging Time at 130°C (hr)	Strain rate mm/min	A	B	C
0	26.2	8/8		
	2.28	8/8		
40	26.2	8/8		
	2.28	6/8	2/8	
100	26.2	6/8	2/8	
	2.28	2/8	3/8	3/8
210	26.2	6/8	1/8	1/8
	2.28	4/8	4/8	
402	26.2	4/8	1/8	3/8
	2.28	3/8	4/8	1/8
600	26.2	4/8	2/8	2/8
	2.28	2/8	4/8	2/8

* the value in the denominator indicate the total number of test samples, while that in the numerator is the no. of samples failed as the specified mode.

The cross-sectional SEM micrograph and X-ray mapping of the as-fired conductor DC2 is given in Fig. 6. Mechanical interlocking between the conductor and the substrate is observed at the conductor/substrate interface. Penetration of the Bi element into the substrate of the conductor/substrate interface is clearly observed, as shown in Fig. 6(d). This suggests the existence of chemical bonding between the conductor and the substrate.

SEM micrographs of the fracture surface of conductor DC1 after 0-, 40-, 100-, 210-, and 400-h aging at 130°C are given in Fig. 7. For this specimen, fracture occurs at the solder/conductor interface. Dimple structure is observed after 40-h aging. The peel strength as a function of aging time for DC1 and DC2 are given in Fig. 8. The peel strength decreases with the aging time initially and then reaches an equilibrium value after 40-h aging for DC2 and after 100-h aging for DC1. Strain rate does not seem to affect the peel strength of either conductor as indicated in Fig. 8.

B. Aging Behavior of Soldered Thick Film Joints

Solder joint failure is classified into three modes. Mode *A* is defined as failure at the conductor/substrate interface. Mode *B* represents a solder/conductor interface failure, and mode *C* is a wire/solder interface failure. Table II summarizes the fail-

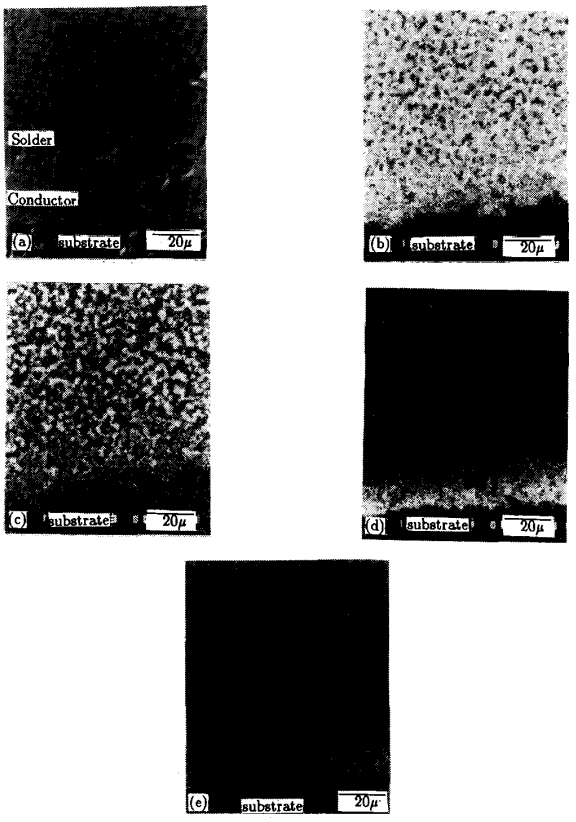

Fig. 9. Cross-sectional view of the sample with conductor DC1, before aging. (a) SEI picture. (b) Sn X-ray mapping. (c) Pb X-ray mapping. (d) Ag X-ray mapping. (e) Pd X-ray mapping.

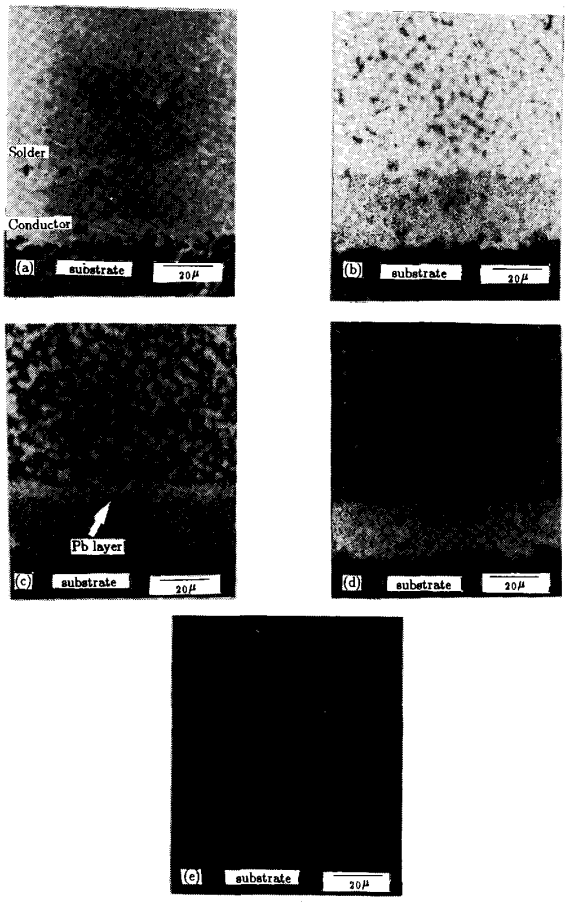

Fig. 10. Cross-sectional view of the sample with conductor DC1 after 100-h aging. (a) SEI picture. (b) Sn X-ray mapping. (c) Pb X-ray mapping. (d) Ag X-ray mapping. (e) Pd X-ray mapping.

ure mode of the conductors after the peel test. For specimens with conductor DC1, the majority of the failures occur at the solder/conductor interface (mode *B*) when aging time is less than 40 h. Mode *A* failure is found for samples aged from 100 to 400 h. However, for specimens with conductor DC2, fracture occurs mostly at the conductor/substrate interface (mode *A*). For samples aged longer than 40 h, some specimens have a mode *B* failure.

The cross-sectional SEM micrographs and X-ray mapping of the soldered specimens before aging and after aging at 130°C for different times are given in Figs. 9 and 10 for conductors DC1 and in Figs. 11–13 for conductor DC2, respectively. Microstructural changes are observed in solder materials after 100-h aging at 130°C. As shown in Figs. 10, 12, and 13, segregation of both Sn-rich and Pb-rich phases occurs as the samples are aged for longer than 100 h. Tin is found in conductor/substrate interface after 100-h aging for conductor DC1 and after 40-h aging for conductor DC2. The 100-h aging time corresponds to the minimum peel strength of samples with conductor DC1, as shown in Fig. 8(a).

C. Adhesion Loss Mechanism

On a system containing a frit-bonded conductor screen printed on a dielectric substrate, Milgram [7] reported that the tin from the Sn/Pb solder replaced the silver at the silver–glass interface and degraded the peel strength. Taylor *et al.* [8] argued that the tin metal from the solder diffused along grain boundaries of the metal and reduced bismuth oxide to bismuth metal. Degradation in adhesion is most severe when the layer of bismuth oxide, i.e., the chemical binder, at the substrate/conductor interface is destroyed. Loasby *et al.* [9] suggests that the volume change caused by tin diffusion into the conductor film and subsequent intermetallic formation degrades the adhesion strength. The X-ray diffraction patterns of 100-h aged samples with conductor DC1, shown in Fig. 14, reveal the existence of alloys Ag_3Sn, Ag_5Sn, Pd_3Sn, Pd_3Sn_2, PdSn, and Pd_2Sn. Fig. 15 gives the X-ray diffraction results of samples with conductor DC2 after 0- 40-, and 210-h thermal aging at 130°C. The XRD data suggests the coexistence of Pd_3Sn, Pd_2Sn, Pd_3Sn_2, PdSn, Ag_5Sn, and Ag_3Sn. The crystal structure, lattice parameter, and unit cell volume of the Pd–Sn and Ag–Sn alloys [10]–[13] are summarized in Table III. The lattice parameter and unit cell volume of conductor DC1 and 4.051 Å and 66.48 Å, respectively.

Conductor/substrate solder/conductor interface failures and minimum peel strength occur when DC1 samples are aged for 100 h and DC2 samples aged for 40 h, as indicated

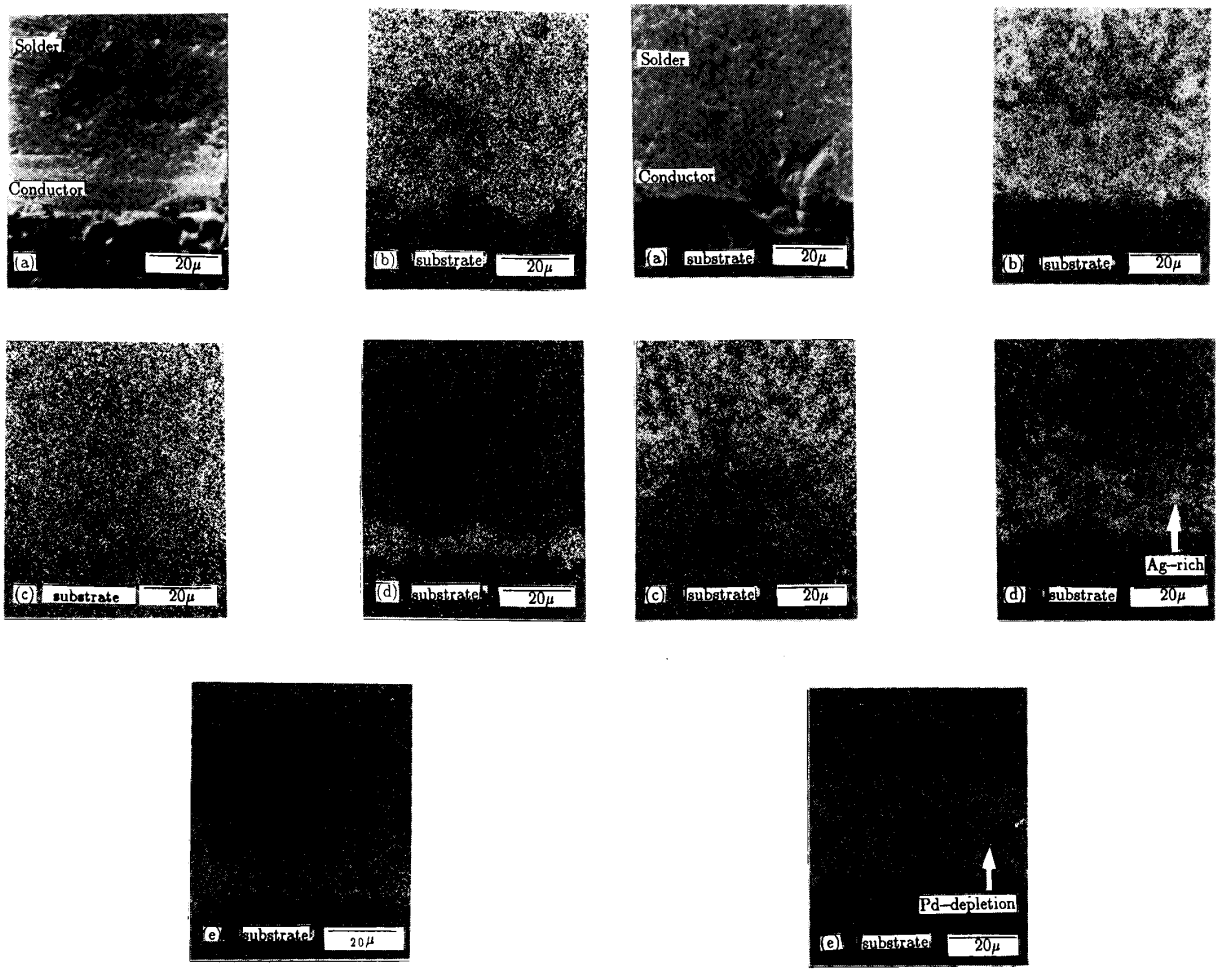

Fig. 11. Cross-sectional view of the sample with conductor DC2 before aging. (a) SEI picture. (b) Sn X-ray mapping. (c) Pb X-ray mapping. (d) Ag X-ray mapping. (e) Pd X-ray mapping.

Fig. 12. Cross-sectional view of the sample with conductor DC2 after 40-h aging. (a) SEI picture. (b) Sn X-ray mapping. (c) Pb X-ray mapping. (d) Ag X-ray mapping. (e) Pd X-ray mapping.

in Table II. Segregation of tin-rich and Pb-rich phases becomes severe, as shown in Figs. 10 and 12. Hence, conductor swelling caused by tin diffusion into the conductor film and volume change caused by subsequent intermetallic formation of Ag_3Sn, Ag_5Sn, Pd_3Sn, PdSn, Pd_2Sn, and Pd_3Sn_2 are the major reasons for the loss of adhesion strength for both conductors.

The oxidation state of the Bi element on the fracture surfaces of the unaged and 40-h aged DC2 samples is investigated by Auger electron spectroscopy. The ESCA results, shown in Figs. 16 and 17, reveal a $4f_{5/2}$ electronic structure of the Bi element. This suggests that Bi element exists in oxide form, Bi_2O_3 [14], [15], instead of metallic form, Bi. This implies that reduction of Bi_2O_3 is not the major cause for the degration of adhesion strength in systems containing conductor DC2.

The room temperature resistivities of elements Pb, Pd, Ag, and Sn are 20.65 $\mu\Omega \cdot$ cm, 10.8 $\mu\Omega \cdot$ cm, 1.59 $\mu\Omega \cdot$ cm, and 11.10 $\mu\Omega \cdot$ cm, respectively [16]. Due to the defect scattering of charge carriers, alloys such as Ag_3Sn, Pd_2Sn, etc, have larger resistivities compared to the constituent components, Ag, Pd, and Sn [17]. The formation of the Pb-rich layer is observed on top of the conductor for DC1 after 100-h aging, shown in Fig. 10(d), and for DC2 after 400-h aging, shown in Fig. 13(c). The larger resistivities of the formed alloy and the Pb-rich layer increase the electrical resistance of the solder joint after aging. The enhanced resistive heating raises the temperature at the solder joint and consequently accelerates the degradation of the solder joints during application.

IV. Summary and Conclusions

1) Intermetallic formation between thick film mixed bonded conductor and Sn/Pb solder is evaluated. The conductor pastes in this study have a Pd:Ag ratios of 1:8 and 1:3 for DC1 and DC2, respectively.

2) Microstructural analysis of the soldered conductor/substrate assembly reveals the existence of mechanical interlocking between conductor and substrate, as well as the penetration of Bi element into the substrate side of the conductor/substrate interface.

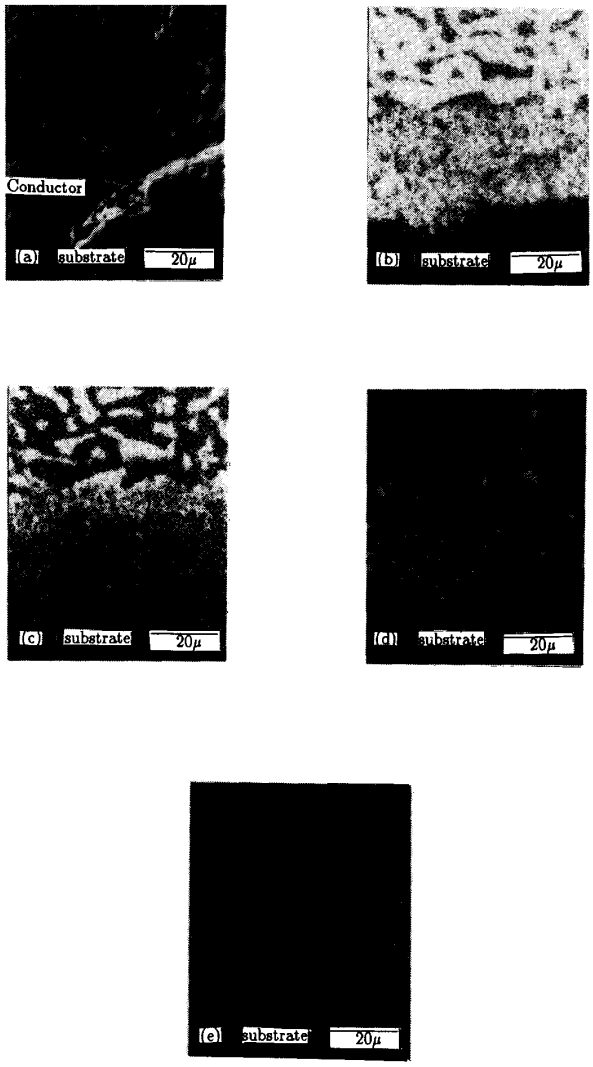

Fig. 13. Cross-sectional view of the sample with conductor DC2 after 400-h aging. (a) SEI picture. (b) Sn X-ray mapping. (c) Pb X-ray mapping. (d) Ag X-ray mapping. (e) Pd X-ray mapping.

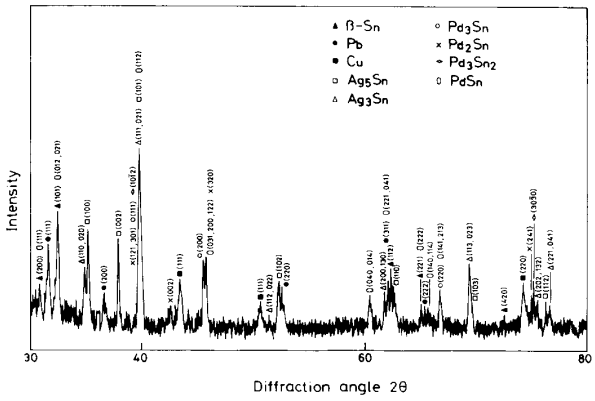

Fig. 14. X-ray diffraction pattern of the sample with conductor DC1 after 100-h aging.

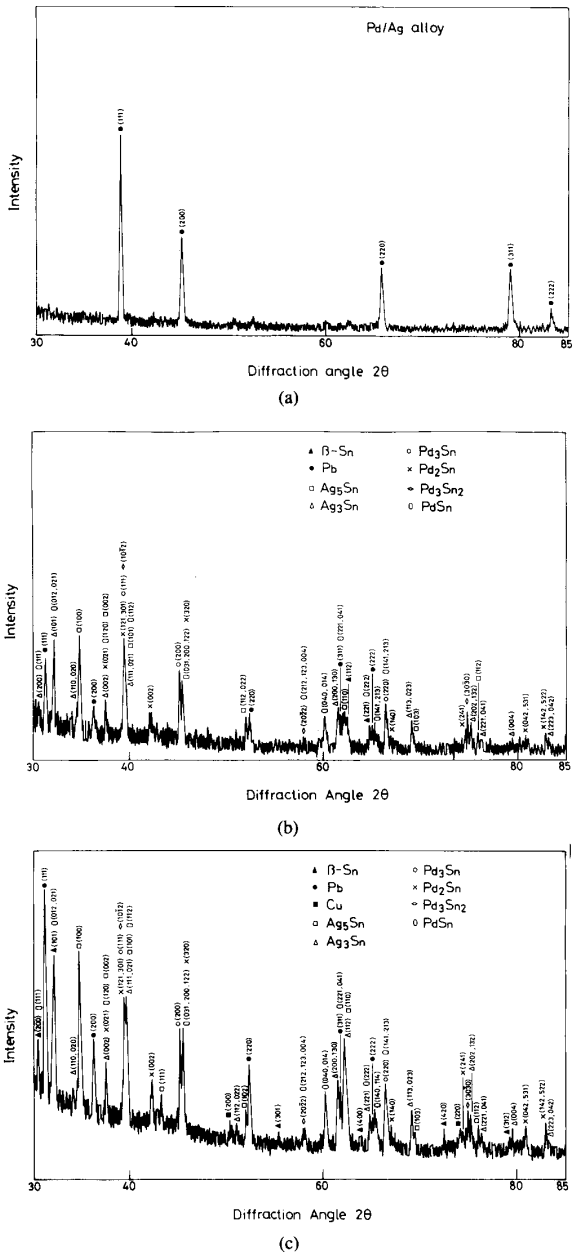

Fig. 15. X-ray diffraction pattern of a sample with conductor DC2 after (a) 0 h; (b) 40 h; (c) 210 h; aging.

3) The decrease in adhesion strength occurs when samples are aged at 130°C for longer than 40 h for DC2 or for longer than 100 h for DC1. Investigation of the microstructure of the Sn/Pb alloy by SEM and EPMA reveals the segregation of Pb-rich and Sn-rich phases in the aged samples. X-ray diffraction results suggest the formation of intermetallic compounds Pd_3Sn_2, Pd_2Sn, Pd_3Sn, PdSn, Ag_5Sn, and Ag_3Sn.

4) Conductor swelling caused by tin diffusion into the conductor film and voltage change caused by the intermetallic formation are the major reasons for the degradation of the

TABLE III
CRYSTAL STRUCTURE, LATTICE PARAMETER, AND UNIT CELL VOLUME OF SOME Pd-Sn AND Ag-Sn ALLOYS

Alloy	Crystal Structure	Lattice Parameter	Unit Cell Volume
Ag_3Sn	orthorhombic	$a_o = 2.995$ Å $b_o = 5.159$ Å $c_o = 4.781$ Å	73.87 Å^3
Ag_5Sn	hexagonal	$a_o = 2.966$ Å $c_o = 4.782$ Å	34.63 Å^3
Pd_2Sn	orthorhombic	$a_o = 8.11$ Å $b_o = 5.662$ Å $c_o = 4.234$ Å	194.42 Å^3
Pd_3Sn_2	hexagonal	$a_o = 4.39$ Å $c_o = 5.655$ Å	94.38 Å^3
Pd_3Sn	face center cubic	$a_o = 3.97$ Å	62.57 Å^3
PdSn	orthorhombic	$a_o = 3.86$ Å $b_o = 6.12$ Å $c_o = 6.31$ Å	149.06 Å^3

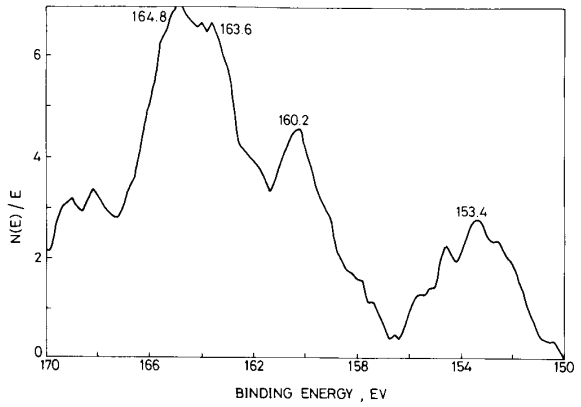

Fig. 16. Multiple scan of Bi in ESCA spectrum for unaged DC2 sample. The major peak at 164.8 corresponds to a $4f_{5/2}$ electronic structure of Bi.

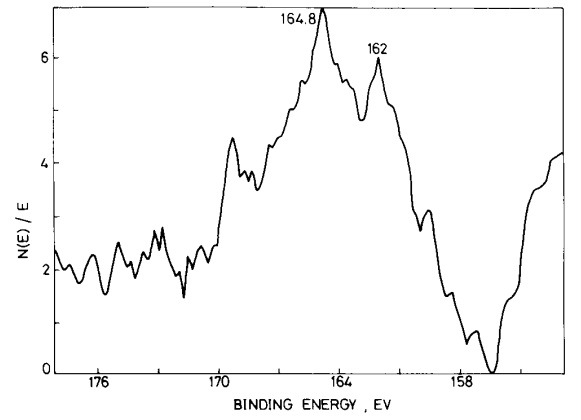

Fig. 17. Multiple scan of Bi in ESCA spectrum for 40 h aged DC2 sample.

peel strength. The reduction of Bi_2O_3 into Bi element is not a major cause in the decrease of the adhesion strength.

5) The high resistivity alloys as well as the Pb-rich layer on top of the conductor may accelerate the degradation of the solder joints.

ACKNOWLEDGMENT

B. S. Chiou appreciates the support and friendship from the Delco Group, General Motor Corporation.

REFERENCES

[1] G. D. O'clock Jr., M. S. Peters, J. R. Patter, G. A. Kleese, and R. V. Martini, "Pb-Sn microstructure: Potential reliability indicator for interconnects," *IEEE Trans. Comp., Hybrids, Manuf. Technol.*, vol. CHMT-10, pp. 82-88, Mar. 1987.

[2] P. W. Dehaven, "The reaction kinetics of liquid 60/40 Sn/Pb solder with copper and nickel: A high temperature X-ray diffraction study," in *Mat. Res. Soc. Symp. Proc.*, vol. 40, 1985, pp. 123-128.

[3] D. S. Dunn, T. F. Marinis, W. M. Sherry, and C. J. Williams, "Dependence of Cu/Sn and Cu/60Sn40Pb solder joint strength on diffusion controlled growth of Cu_3Sn and Cu_6Sn_5," in *Mat. Res. Soc. Symp. Proc.*, vol. 40, 1985, pp. 129-138.

[4] C. W. Allen, M. R. Fulcher, A. S. Rai, G. A. Sargent, and A. E. Miller, "A study of intermetallic compound development in nickel—Tin interfacial zones," in *Mat. Res. Soc. Symp. Proc.*, vol. 40, 1985, pp. 139-144.

[5] B. D. Cullity, *Elements of X-ray Diffraction*, 2nd ed. Reading, MA: Addison-Wesley, 1978, p. 356.

[6] I. Karakaya and W. T. Thompson, *Bull. Alloy Phase Diagram*, vol. 9, no. 3, p. 23, 1988.

[7] A. A. Milgram, "Influence of metallic diffusion on the adhesion of screen printed silver films," *Metallurgical Trans.*, vol. 1, pp. 695-700, 1970.

[8] B. E. Taylor, J. J. Felten, and J. R. Larry, "Progress in and technology of low-cost silver containing thick film conductors," *IEEE Trans. Comp., Hybrids, Manuf. Technol.*, vol. CHMT-3, pp. 504-517, 1980.

[9] R. G. Loasby, N. Davey, and H. Barlow, "Enhanced property thick-film conductor pastes," *Solid-State Technol.*, pp. 46–50, 1972.
[10] I. R. Harris and M. Cordey-Hayes, "A study of some palladium-tin, silver-tin and palladium-silver-tin alloy," *J. Less-Common Metals*, vol. 16, pp. 223–232, 1968.
[11] H. W. King and T. B. Massalski, "Lattice spacing relationships and the electronic structure of the H.C.P. ζ phases based on silver," *Philosoph. Mag.*, pp. 669–682, 1960.
[12] O. Nial, A. Almin, and A. Westgren, "Rönttgenanalyse der Systeme Gold-Antimon und Silber-Zinn," *Z. Phzsikal. Chem.*, vol. 138, pp. 81–90, 1931.
[13] M. Hanson and K. Anderko, eds., *Constitution of Binary Alloys,* New York: McGraw-Hill, 1958; *1st Supplement*, R. P. Elliott, Ed. New York: McGraw-Hill, 1965.
[14] T. P. Debies and J. W. Rabalais, "X-ray photoelectron spectra and electronic structure of Bi_2X_3 (x = O, S, Se, Te)," *Chem. Phys.*, vol. 20, pp. 277–283, 1977.
[15] W. E. Morgan, W. J. Stec, and J. R. Van Wazer, "Inter-orbital binding-energy shifts of antimony and bismuth compounds," *Inorgan. Chem.*, vol. 12, no. 2, pp. 953–955, 1973.
[16] *CRC Handbook of Chemistry and Physics*, R. C. Weast, Ed. Boca Raton, FL: CRC, 1980.
[17] R. W. Berry, P. M. Hall, and M. T. Harris, *Thin Film Technology,* New York: Van Nostrand Reinhold, 1982, pp. 303–307.